

# GSplatLoc: Grounding Keypoint Descriptors into 3D Gaussian Splatting for Improved Visual Localization<sup>†</sup>

Gennady Sidorov<sup>1,2</sup>, Malik Mohrat<sup>1,2</sup>, Ksenia Lebedeva<sup>1</sup>, Ruslan Rakhimov<sup>2</sup>, and Sergey Kolyubin<sup>1</sup>

**Abstract**—Although various visual localization approaches exist, such as scene coordinate and pose regression, these methods often struggle with high memory consumption or extensive optimization requirements. To address these challenges, we utilize recent advancements in novel view synthesis, particularly 3D Gaussian Splatting (3DGS), to enhance localization. 3DGS allows for the compact encoding of both 3D geometry and scene appearance with its spatial features. Our method leverages the dense description maps produced by XFeat’s lightweight keypoint detection and description model. We propose distilling these dense keypoint descriptors into 3DGS to improve the model’s spatial understanding, leading to more accurate camera pose predictions through 2D-3D correspondences. After estimating an initial pose, we refine it using a photometric warping loss. Benchmarking on popular indoor and outdoor datasets shows that our approach surpasses state-of-the-art Neural Render Pose (NRP) methods, including NeRFMatch and PNeRFLoc. Project page: <https://gsplatloc.github.io>.

## I. INTRODUCTION

Visual localization is a crucial task in computer vision that involves determining the pose (position and orientation) of a moving camera relative to a predefined environment map. This capability is essential for machines to understand their position within a 3D space and forms a foundational component in Simultaneous Localization and Mapping (SLAM) and Structure from Motion (SfM) systems. It also supports a range of practical applications, including mobile manipulation, autonomous driving, and augmented/virtual reality (AR/VR) experiences [1], [2].

Early methods for visual re-localization used image retrieval techniques. These approaches involved comparing a query image with a database of photos with known camera poses to approximate the environment’s representation. The pose of the query image was inferred by identifying the closest match in the database. While straightforward, these methods often struggled with scalability and accuracy.

Subsequent methods employed structured approaches, such as sparse feature matching. In these methods, a global map of 3D points was used to find correspondences between 2D feature points extracted from the query image and 3D points in the map. These techniques are known for their robustness, scene agnosticism, and high accuracy, even with short query times. However, they face challenges due to their



Fig. 1: *GSplatLoc* constructs a 3D Gaussian Splatting (3DGS) model with distilled descriptor features. For localization, the initial coarse pose is estimated through structural matching with these features and refined during test-time optimization using rendering-based photometric warp loss to enhance accuracy.

significant memory requirements, especially in large-scale environments [3].

Pose regression methods introduced the use of neural networks to predict the pose from a query image. By integrating the environmental map into the network’s architecture, these methods enabled end-to-end training without requiring a detailed 3D structure of the environment. However, they often lag behind structured methods in pose accuracy [4]. Absolute Pose Regression (APR) techniques offer high-quality pose estimations while addressing memory and time constraints. Scene Coordinate Regression (SCR) further refines this by optimizing small-sized maps to implicitly learn the scene and match input pixel locations with their 3D counterparts. This approach achieves accuracy comparable to structured methods but suffers from lengthy optimization processes.

Recent advancements have explored neural-based 3D representations, such as Neural Radiance Fields (NeRF) [5] and 3D Gaussian Splatting (3DGS) [6]. These methods enhance localization by synthesizing new images from various views as a data augmentation step during training. They improve performance by encoding both 3D geometry and the appearance of the environment. Some methods establish correspondences between the query image and its rendered counterpart, but they often face issues with artifacts in

<sup>†</sup>This work has been submitted to the IEEE for possible publication. Copyright may be transferred without notice, after which this version may no longer be accessible.

<sup>1</sup> BE2R Lab, ITMO University, St. Petersburg, Russia. {gksidorov, mmohrat, klebedeva, s.kolyubin}@itmo.ru

<sup>2</sup> Robotics Center, Moscow, Russia.

rendered images. Enhancements such as adding descriptive features to NeRFs have improved robustness against these artifacts and pose estimation accuracy [7], [8], [9], [10]. GSLoc [11] uses 3DGS solely as a test-time refinement framework to improve the accuracy of poses estimated by a standalone pose estimator.

Addressing these limitations, we introduce a novel framework, GSplatLoc, for visual localization that integrates structure-based coarse pose estimation and rendering-based optimization in a single pipeline. Our approach utilizes a point-based 3D Gaussian Splatting (3DGS) representation to distill scene-agnostic feature descriptors for initial coarse pose estimation and refine it as shown in Figure 1. Specifically, our pipeline estimates a coarse pose by matching 2D descriptors with 3D features distilled into 3D Gaussians during scene modeling. It also supports pose refinement through rendering-based optimization by aligning rendered and query images and minimizing a photometric warping loss function. This method addresses the limitations of traditional approaches and significantly improves accuracy.

Our main contributions are:

- We propose a novel visual re-localization pipeline using 3DGS, which enables structure-based feature matching for accurate pose estimation.
- We demonstrate how distilling local feature descriptors into the representation allows for accurate coarse pose estimation.
- We show that 3DGS’s ability to quickly render photo-realistic images facilitates effective camera pose refinement.

## II. RELATED WORK

### A. Structure-Based Localization Methods

Structure-based approaches use 3D scene information from Structure-from-Motion (SfM) to register a query image from the same scene via explicit 2D-3D correspondences, typically employing the PnP algorithm with RANSAC. While these methods can achieve high accuracy in pose estimation, they are sensitive to noisy correspondences [12], [13].

Scene coordinate regression (SCR) methods, a subset of structure-based approaches, also offer high accuracy. These methods regress 3D scene coordinates onto 2D images, allowing the use of reprojection error for pose estimation [14], [15]. In these models, the environment is represented by a trainable function that predicts dense correspondence fields between images and scenes. Neural networks can regress 2D-3D correspondences to serve as inputs for pose optimization using RANSAC. These methods may use random forest models [16], [17], convolutional neural networks with RGB-D input [18], [19], [20], or solely RGB images, as in ACE [15].

In our paper, we show that it is feasible to extend further the accuracy of structure-based models with a simple, yet effective method to firstly find a coarse camera pose and then refine the estimated pose by utilizing feature fields stored in the map representation of 3D Gaussians.

### B. Keypoints Description and Matching Models

Recent advancements utilize Convolutional Neural Networks (CNNs) to enhance sparse detectors and local descriptors [21], [22], [23]. Some works draw on transformer architectures to improve the spatial relationship between key points and their visual appearance. Although transformer-based models offer robustness, they are computationally expensive. To address this, more efficient architectures have been proposed [24], [25]. For instance, XFeat [26] is a lightweight CNN-based feature extractor that produces compact dense descriptors and is trained on large-scale datasets with pixel-level ground truth correspondences. Feature matching-based localization methods have employed these networks for deep feature matching and pose refinement [27], [10], [28]. In our work, we chose the XFeat model to balance computational efficiency with accuracy.

### C. Localization Based on Novel View Synthesis

NeRF [5] can generate high-quality images from new perspectives, which can be used for localization tasks. Algorithms such as DFNet [28] and NeFeS [10] use feature extractors to optimize differences between synthesized and reference images. Subsequent methods like iNeRF [29] refine pose estimation through an inverted NeRF task, and Direct-PN [30] uses NeRF as a direct matching module to compute photometric loss between synthesized and query images.

Recently, NeRF models have been extended to synthesize and render feature fields along with radiance fields. These feature fields are typically learned through supervision from 2D feature extractors using volumetric rendering. Works such as [8], [7] have shown that 3D feature fields outperform 2D baselines in tasks like 3D segmentation and visual localization. For example, PNeRFLoc [31] improves pose estimation accuracy by minimizing warping loss for pixel alignment. NeRFMatch [32] enhances positioning by finding 2D-3D matches with specialized feature extractors. However, these methods require extensive training and rendering time.

Conversely, the 3DGS [6] approach represents scenes using differentiable 3D Gaussians. Methods like iComMa [33] integrate matching and comparison losses between rendered and query images to improve pose estimation robustness. GSLoc [11] refines pre-estimated poses from external pose extractors during test time.

In our paper, we explore distilled neural feature fields from scene-agnostic keypoint detector and descriptor models for the camera re-localization task. We demonstrate their role in providing pose prior and refining pose during test time, utilizing the advantages of 3D-GS such as explicit map representation and fast rendering speed.

## III. PRELIMINARIES

Our method integrates keypoint descriptor models with 3D Gaussian Splatting, combining keypoint features into the 3D representation to improve re-localization accuracy. We outline this process briefly.

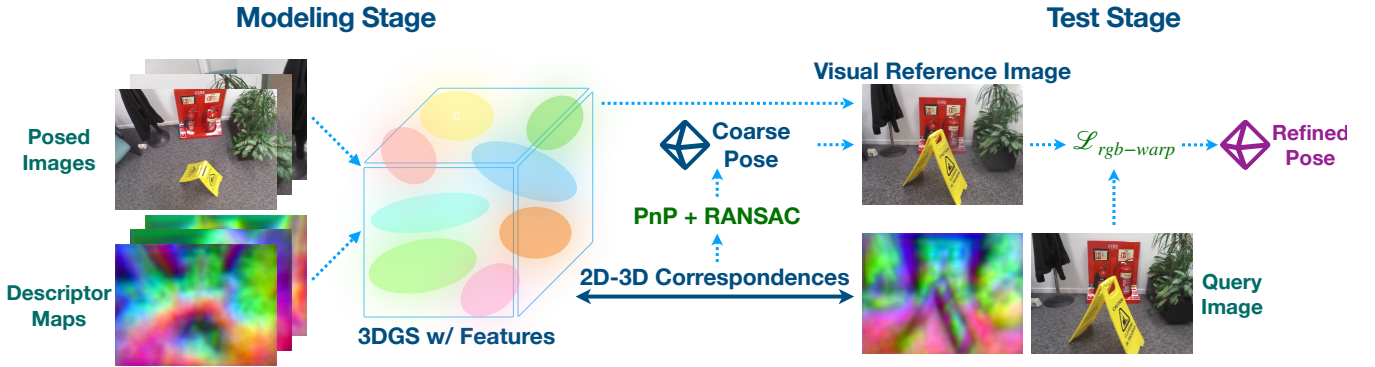


Fig. 2: Overview of the GSplatLoc pipeline. First, we model the scene using a feature-based 3D Gaussian Splatting (3DGS) approach, supervised by the XFeat [26] network to extract and distill features. In the test stage, the initial coarse pose is estimated by matching 2D keypoints from the query image to 3D features in the 3DGS model followed by a Perspective-n-Point (PnP) solver within a RANSAC loop. We then refine the coarse pose by aligning a rendered image with the input query image using a RGB warping loss. This process improves pose accuracy through test-time optimization.

#### A. Feature Distillation into 3D Gaussian Splatting

Building on the Feature-3DGS framework [9], we employ a modified 3DGS to distill high-dimensional features into a feature field, alongside a radiance field. This technique uses parallel N-dimensional Gaussian rasterization and a speed-up module, making it compatible with various 2D foundation models.

We initialize the 3D Gaussians using a point cloud from an SfM model. Their projection into 2D space involves transforming covariance matrices and incorporating rotation, scaling, opacity, spherical harmonics, color, and other visual features.

Pixel color and feature values are computed through  $\alpha$ -blending, supervised by a "teacher" model, using differentiable rendering for distillation. The joint optimization method rasterizes both RGB images and feature maps simultaneously, ensuring high fidelity and per-pixel accuracy. The optimizable attributes of the  $i$ -th 3D Gaussian  $\Psi_i$  are:

$$\Psi_i = \{y_i, q_i, s_i, \alpha_i, c_i, f_i\}, \quad (1)$$

where  $y_i \in \mathbb{R}^3$  represents the 3D position,  $q_i \in \mathbb{R}^4$  denotes the rotation quaternion,  $s_i \in \mathbb{R}$  is the scaling factor,  $\alpha_i \in \mathbb{R}$  is the opacity value,  $c_i \in \mathbb{R}^3$  represents the diffuse color from Spherical Harmonics (SH), and  $f_i \in \mathbb{R}^V$  is the feature embedding from the supervised model  $F_t$ , where  $V$  denotes the dimension of the feature vector. Each Gaussian  $\Psi_i$  is thus positioned at  $y_i$  with a feature vector  $f_i$  that encodes local spatial and visual content.

The following equations define the computation of pixel color  $C$  and pixel feature  $F_r$  during rendering:

$$C = \sum_{i \in \mathcal{N}} c_i \alpha_i T_i, \quad F_r = \sum_{i \in \mathcal{N}} f_i \alpha_i T_i, \quad (2)$$

where  $\mathcal{N}$  represents the set of overlapping 3D Gaussians for a given pixel, and  $T_i$  denotes the transmittance, which is the product of the opacity values of previous Gaussians overlapping the same pixel.

To train the 3DGS model for a specific scene with grounded feature maps, we use the loss function  $\mathcal{L}_{GS}$ , which combines photometric loss  $\mathcal{L}_{color}$  and feature loss  $\mathcal{L}_{features}$ . The photometric loss  $\mathcal{L}_{color}$  consists of  $\mathcal{L}_1$  and  $\mathcal{L}_{SSIM}$  losses between the ground truth image  $I$  and the rendered image  $\hat{I}$ , while  $\mathcal{L}_{features}$  measures the difference between the supervised feature map  $F_t(I)$  and the rendered feature map  $F_r$ :

$$\mathcal{L}_{GS} = \mathcal{L}_{color} + \mathcal{L}_{features}, \quad (3)$$

where:

$$\begin{aligned} \mathcal{L}_{color} &= (1 - \lambda)\mathcal{L}_1(I, \hat{I}) + \lambda\mathcal{L}_{SSIM}(I, \hat{I}), \\ \mathcal{L}_{features} &= \|F_t(I) - F_r\|_1. \end{aligned}$$

## IV. METHODOLOGY

Our method comprises a two-stage pipeline, as depicted in Figure 2. The first stage involves modeling the scene, and the second stage focuses on estimating an initial coarse pose and refining it for improved accuracy.

Initially, we model the scene using a feature-based 3D Gaussian Splatting (3DGS) approach [9], guided by a key-point descriptor network. We utilize the deep feature extractor XFeat [26] due to its robustness in extracting reliable and distinctive features across various environments, both indoor and outdoor, even in the presence of dynamic elements.

For each reference image  $I_t \in \mathbb{R}^{W \times H \times 3}$ , the XFeat network computes a feature map  $F_t(I) \in \mathbb{R}^{(W/8) \times (H/8) \times 64}$ , which is bilinearly upsampled to the full resolution. We train the 3D Gaussian Splatting model by minimizing the loss function described in Equation 3.

Once the scene is learned by 3DGS, we estimate the pose for the query image through a two-step process: initially estimating a coarse pose and then refining it.



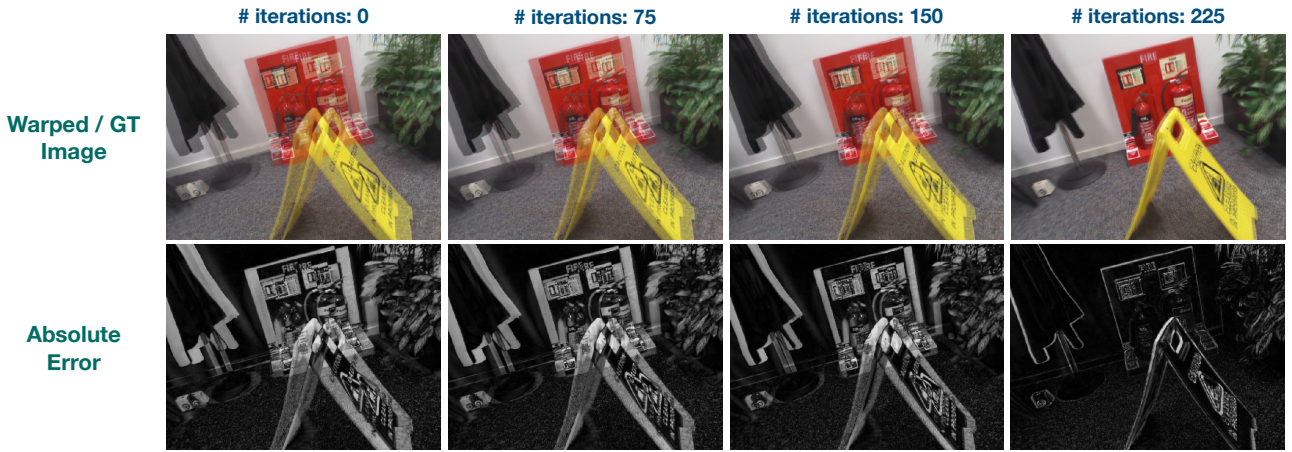


Fig. 3: *Test-time camera pose refinement* aligns the rendered images with the query image at different optimization iterations. The first row shows the rendered images blended with the query image based on the estimated pose at each step, while the second row visualizes the absolute error between the two, demonstrating how the warping loss reduces this error over time and improves pose accuracy.

*a) Obtaining the Initial Coarse Pose:* This stage aims to establish correspondences between 2D keypoints in the query image and 3D points in the 3DGS model of the scene. We use a Perspective-n-Point (PnP) solver within a RANSAC loop to provide an initial pose estimate.

For a given query image  $q$  with extracted keypoints  $P_q$  and features  $f_q$  from a descriptor model, we perform 2D-3D correspondence matching with the 3D Gaussian point cloud  $P \in \mathbb{R}^{N \times 3}$  and the associated distilled XFeat features  $f_p \in \mathbb{R}^{N \times 64}$ , where  $N$  denotes the number of points. Following the PNeRFLoc method [31], we use cosine similarity to match the 2D query image features with the 3D scene features distilled in the 3D Gaussians. The 2D-3D correspondences  $V(i)$  for each  $i$ -th pixel are determined by maximizing this measure:

$$V(i) = \arg \max_{i \in P} \frac{\mathbf{f}_q^i \cdot \mathbf{f}_p^i}{\|\mathbf{f}_q^i\| \|\mathbf{f}_p^i\|}, \quad (4)$$

While PNeRFLoc accelerates the search by learning a reliability score for each point and filtering based on this score, we use only the sparse, reliable keypoints from the query image extracted by XFeat and *all* points in the point cloud. This approach supports accurate and efficient pose estimation through semi-dense matching between the query image and the Gaussian cloud of distilled features.

*b) Test-time Camera Pose Refinement:* We refine the coarse pose estimate by aligning the rendered image with the input query image.

Previous works [34], [35] used gradient descent to minimize photometric residuals, requiring neural rendering at each step. PNeRFLoc [31] improved this by introducing a warping loss function that requires rendering only once. We adopt this warping loss approach. Additionally, the 3DGS framework enhances speed with its faster rendering process compared to PNeRFLoc.

For a given query image  $q$  and an initial coarse pose

$(\mathbf{R}, \mathbf{t})$ , GSplatLoc first renders an image  $q_r$  and a depth map  $d_r$  using the initial pose. We aim to optimize the pose estimate  $(\mathbf{R}', \mathbf{t}')$  by minimizing a warping loss, defined as the sum of pixel-wise RGB differences between the reference and query images:

$$\mathcal{L}_{rgb-warp} = \sum_{p_i} \|C(q, W(p_i, \mathbf{R}, \mathbf{t}, \mathbf{R}', \mathbf{t}')) - C(q_r, p_i)\|_2, \quad (5)$$

$$W(p_i, \mathbf{R}, \mathbf{t}, \mathbf{R}', \mathbf{t}') = \prod (\mathbf{R}'(\mathbf{R}^{-1} \prod^{-1}(p_i, d_r(p_i)) - \mathbf{R}^{-1}\mathbf{t}) + \mathbf{t}'), \quad (6)$$

Here,  $C(q_r, p_i) \in \mathbb{R}^3$  is the RGB color at pixel  $p_i \in \mathbb{R}^2$  on the rendered image  $q_r$ , and the warp function  $W(\cdot)$  finds the corresponding pixel on the query image  $q$  by warping  $p_i$  from the reference image  $q_r$ . Specifically,  $W$  back-projects  $p_i$  into the 3D space of the camera coordinate system of  $q_r$  using the rendered depth  $d_r$ , transforms it to the camera coordinate system of  $q$  using the optimized pose  $(\mathbf{R}', \mathbf{t}')$ , and then projects it onto the image  $q$ .

## V. EXPERIMENTS

To evaluate our work, we use the 7Scenes dataset [42] for indoor validation and the Cambridge Landmarks dataset [36] for outdoor validation.

During the modeling phase, we use COLMAP [43] to create point clouds and initialize poses for each scene in these datasets. We then train the 3D Gaussian Splatting (3DGS) model from [9] on each scene for 15,000 iterations. XFeat [26] extracts dense features to be used in 3DGS.

In the testing phase, we start by obtaining an initial coarse pose. We sample 1,000 of the most reliable descriptors and match them with the 3D feature cloud. We set the number of RANSAC iterations to 20,000.

For the refinement step, we render a visual reference for the coarse pose once and use the Adam optimizer with a

TABLE I: *Comparison of Methods on the 7Scenes Dataset.* The table reports the median translation and rotation errors (cm/°) for various methods. APR stands for absolute pose regression, SCR for scene coordinate regression, and NRP for neural render pose estimation. The best results are highlighted in **first** and **second**.

	Methods	Chess	Fire	Heads	Office	Pumpkin	Redkitchen	Stairs	Avg. ↓ [cm/°]
APR	PoseNet [36]	10/4.02	27/10.0	18/13.0	17/5.97	19/4.67	22/5.91	35/10.5	21/7.74
	MS-Transformer [37]	11/6.38	23/11.5	13/13.0	18/8.14	17/8.42	16/8.92	29/10.3	18/9.51
	DFNet [28]	3/1.12	6/2.30	4/2.29	6/1.54	7/1.92	7/1.74	12/2.63	6/1.93
	Marepo [38]	1.9/0.83	2.3/0.92	2.1/1.24	2.9/0.93	2.5/0.88	2.9/0.98	<b>5.9</b> / 1.48	2.9/1.04
SCR	ACE [15]	<b>0.5</b> / <b>0.18</b>	<b>0.8</b> / <b>0.33</b>	<b>0.5</b> / <b>0.33</b>	<b>1.0</b> / <b>0.29</b>	<b>1</b> / <b>0.22</b>	<b>0.8</b> / <b>0.2</b>	<b>2.9</b> / <b>0.81</b>	<b>1.1</b> / <b>0.34</b>
NRP	FQN-MN [39]	4.1/1.31	10.5/2.97	9.2/2.45	3.6/2.36	4.6/1.76	16.1/4.42	139.5/34.67	28/7.3
	CrossFire [40]	1/0.4	5/1.9	3/2.3	5/1.6	3/0.8	2/0.8	12/1.9	4.4/1.38
	PNeRFLoc [31]	2/0.8	2/0.88	<b>1.0</b> / 0.83	3/1.05	6/1.51	5/1.54	32/5.73	7.28/1.76
	NeRFMatch [32]	0.9/0.3	1.3/0.4	1.6/1.0	3.3/0.7	3.2/0.6	<b>1.3</b> / <b>0.3</b>	7.2/ <b>1.3</b>	2.7/0.7
	<b>GSplatLoc (Coarse)</b>	3.17/0.49	3.34/0.7	1.96/0.76	3.8/0.62	5.12/0.7	4.54/0.64	10.97/2.63	4.7/0.94
	<b>GSplatLoc (Fine)</b>	<b>0.43</b> / <b>0.16</b>	<b>1.03</b> / <b>0.32</b>	1.06/ <b>0.62</b>	<b>1.85</b> / <b>0.4</b>	<b>1.8</b> / <b>0.35</b>	2.71/0.55	8.83/2.34	<b>2.53</b> / <b>0.68</b>

TABLE II: *Comparisons on Cambridge Landmarks dataset.* The table reports the median translation and rotation errors (cm/°) for various methods. APR stands for absolute pose regression, SCR for scene coordinate regression, and NRP for neural render pose estimation. The best results are highlighted in **first** and **second**.

	Methods	Kings	Hospital	Shop	Church	Avg. ↓ [cm/°]
APR	PoseNet	93/2.73	224/7.88	147/6.62	237/5.94	175/5.79
	MS-Transformer	85/1.45	175/2.43	88/3.20	166/4.12	129/2.80
	LENS [41]	33/0.5	44/0.9	27/1.6	53/1.6	39/1.15
	DFNet	73/2.37	200/2.98	67/2.21	137/4.02	119/2.90
SCR	ACE	29/0.38	31/ <b>0.61</b>	<b>5</b> / <b>0.3</b>	<b>19</b> / <b>0.6</b>	<b>21</b> / <b>0.47</b>
NRP	FQN-MN [39]	<b>28</b> / <b>0.4</b>	54/0.8	13/0.6	58/2	38/1
	CrossFire	47/0.7	43/0.7	20/1.2	39/1.4	37/1
	PNeRFLoc [31]	<b>24</b> / <b>0.29</b>	<b>28</b> / <b>0.37</b>	<b>6</b> / <b>0.27</b>	40/ <b>0.55</b>	24.5/ <b>0.37</b>
	<b>GSplatLoc (Coarse)</b>	41/0.50	32/0.87	11/0.40	31/0.72	29/0.62
	<b>GSplatLoc (Fine)</b>	<b>27</b> / 0.46	<b>20</b> / 0.71	<b>5</b> / 0.36	<b>16</b> / 0.61	<b>17</b> / 0.53

learning rate of 0.001. We optimize both translation and rotation in quaternion form. Figure 3 shows that our rendering-based optimization gradually improves localization accuracy from the initial coarse pose, with about 250 iterations needed for indoor scenes and 350 for outdoor scenes while we render the visual reference process only once.

We compare our results with several state-of-the-art methods and report the median translation and rotation errors (in cm/degree) for each scene and the average for all scenes in Tables I and II for both coarse and fine poses.

For the indoor 7Scenes dataset, our method, GSplatLoc, outperforms the previous state-of-the-art NeRFMatch in five out of seven scenes and sets a new state-of-the-art among neural rendering-based pose estimation methods. However, GSplatLoc is still outperformed by ACE, a scene coordinate regression method.

On the outdoor Cambridge Landmarks dataset, which includes dynamic objects and light variations, GSplatLoc performs the best. It even surpasses ACE, the second-best method, by an average of 4 cm in translation error while matching ACE’s performance in rotation error.

We present the optimization process of the estimated

coarse pose in Figure 4, where the first point represents the average coarse pose value across the Cambridge scene. Based on our experiments, the optimal number of iterations for the Cambridge scene is 350, using early stopping. Beyond this point, the warp loop can begin to overfit on artifacts, increasing in translation error.

Table III shows the execution time of our method on the 7Scenes dataset. The minimum time is spent searching for the coarse pose and rendering, while the longest time, around 2.7 seconds, is taken by the iterative process of refining with warp loss over 250 iterations. Runtime analysis experiments were conducted on an Nvidia RTX 4060 Ti GPU. Our method can achieve a speed of 2-3 fps when maximum accuracy is not a priority. Therefore, there may be a tradeoff between execution speed and refinement quality by reducing the number of iterations.

## Discussion on results

Our method achieves state-of-the-art performance among neural rendering pose estimation (NRP) methods in both indoor and outdoor scenarios, although it performs slightly worse than ACE in indoor environments.

We argue that there are two reasons for this. First, feature distillation combined with 3DGS enables accurate structure-based coarse pose estimation. Second, representations that provide realistic images facilitate effective photometric optimization.

In contrast, ACE, a scene coordinate regression (SCR)-based pose estimation method, struggles with outdoor scenarios due to its limited modeling capabilities, constrained by its shallow MLP-based scene encoding design.

Overall, NRP is a more versatile framework than SCR, as it allows solving multiple tasks in parallel using the same scene representation. For example, 3DGS can be used to encode semantic or language-aligned instances or even model dynamic scenes—tasks that are crucial in robotics. This flexibility enables a broader range of interactions with the environment and enhances localization.

One key advantage of our proposed pipeline is its speed. It

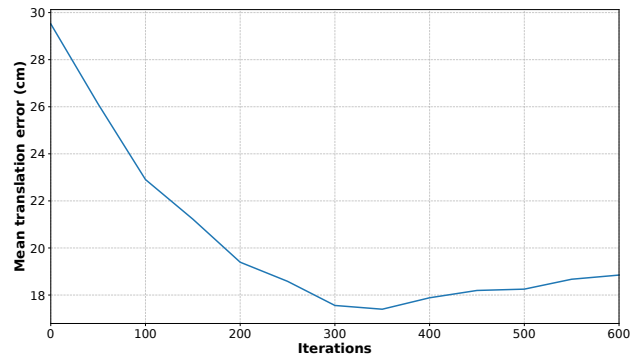
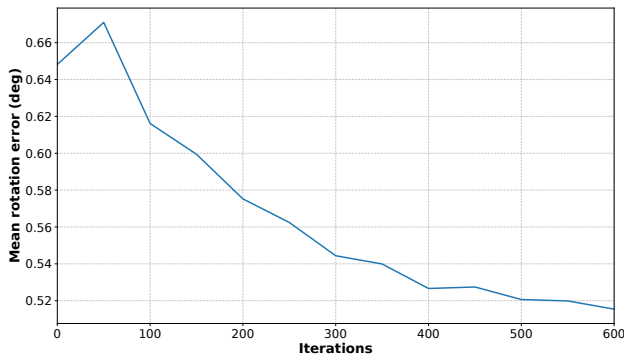


Fig. 4: We optimize the camera pose using rendering-based photometric warp loss, which iteratively reduces translation (cm) and rotation (degrees) errors. The plots illustrate the average error reduction across scenes in the Cambridge Landmarks dataset.

TABLE III: Runtime analysis of the execution time per frame for each stage of our method on the 7Scenes dataset.

Stage	Avg. ↓ time(s)
Establishing 2D-3D matches	0.144
Rendering	0.152
Warp loss	2.715

requires only 0.3 seconds to estimate an initial coarse pose, compared to around 3 seconds in the PNeRFLoc [31].

While not explored in this paper, we anticipate that our method could further improve by removing floaters from the trained 3DGS model.

## VI. CONCLUSION

In this paper, we demonstrate how to leverage the powerful 3D Gaussian Splatting (3DGS) scene representation and introduce the GSplatLoc framework for accurate and efficient pose estimation and refinement. By incorporating structure-based feature matching with rendering-based optimization, our approach estimates an initial pose without relying on a separate pose estimator. The proposed framework’s ability to extract scene-agnostic descriptors from 3DGS enhances pose estimation quality. This unified method estimates the initial pose through 2D-3D correspondences and refines it by minimizing warping loss between the query and rendered images.

Future work may focus on more challenging, large-scale outdoor scenarios where 3DGS has already shown promising results. Extensions such as CityGaussian [44] or VastGaussian [45] could be valuable avenues for exploration.

## REFERENCES

- [1] Z. Dong, G. Zhang, J. Jia, and H. Bao, “Keyframe-based real-time camera tracking,” in *2009 IEEE 12th International Conference on Computer Vision*, 2009, pp. 1538–1545.
- [2] L. Heng, B. Choi, Z. Cui, M. Geppert, S. Hu, B. Kuan, P. Liu, R. Nguyen, Y. C. Yeo, A. Geiger, G. H. Lee, M. Pollefeys, and T. Sattler, “Project autovision: Localization and 3d scene perception for an autonomous vehicle with a multi-camera system,” 2019. [Online]. Available: <https://arxiv.org/abs/1809.05477>
- [3] H. Lim, S. N. Sinha, M. F. Cohen, and M. Uyttendaele, “Real-time image-based 6-dof localization in large-scale environments,” in *2012 IEEE Conference on Computer Vision and Pattern Recognition*, 2012, pp. 1043–1050.
- [4] P.-E. Sarlin, A. Unagar, M. Larsson, H. Germain, C. Toft, V. Larsson, M. Pollefeys, V. Lepetit, L. Hammarstrand, F. Kahl, and T. Sattler, “Back to the Feature: Learning Robust Camera Localization from Pixels to Pose,” in *CVPR*, 2021.
- [5] B. Mildenhall, P. P. Srinivasan, M. Tancik, J. T. Barron, R. Ramamoorthi, and R. Ng, “Nerf: Representing scenes as neural radiance fields for view synthesis,” 2020.
- [6] B. Kerbl, G. Kopanas, T. Leimkühler, and G. Drettakis, “3d gaussian splatting for real-time radiance field rendering,” 2023.
- [7] V. Tschernezki, I. Laina, D. Larlus, and A. Vedaldi, “Neural feature fusion fields: 3d distillation of self-supervised 2d image representations,” 2022.
- [8] S. Kobayashi, E. Matsumoto, and V. Sitzmann, “Decomposing nerf for editing via feature field distillation,” 2022.
- [9] S. Zhou, H. Chang, S. Jiang, Z. Fan, Z. Zhu, D. Xu, P. Chari, S. You, Z. Wang, and A. Kadambi, “Feature 3dgs: Supercharging 3d gaussian splatting to enable distilled feature fields,” *arXiv preprint arXiv:2312.03203*, 2023.
- [10] S. Chen, Y. Bhalgat, X. Li, J. Bian, K. Li, Z. Wang, and V. A. Prisacariu, “Neural refinement for absolute pose regression with feature synthesis,” 2024.
- [11] C. Liu, S. Chen, Y. Bhalgat, S. Hu, Z. Wang, M. Cheng, V. A. Prisacariu, and T. Braud, “Gslloc: Efficient camera pose refinement via 3d gaussian splatting,” *arXiv preprint arXiv:2408.11085*, 2024.
- [12] W. Cheng, W. Lin, K. Chen, and X. Zhang, “Cascaded parallel filtering for memory-efficient image-based localization,” 2019. [Online]. Available: <https://arxiv.org/abs/1908.06141>
- [13] C. Toft, E. Stenborg, L. Hammarstrand, L. Brynte, M. Pollefeys, T. Sattler, and F. Kahl, “Semantic match consistency for long-term visual localization,” in *Computer Vision – ECCV 2018*, V. Ferrari, M. Hebert, C. Sminchisescu, and Y. Weiss, Eds. Cham: Springer International Publishing, 2018, pp. 391–408.
- [14] E. Brachmann, A. Krull, S. Nowozin, J. Shotton, F. Michel, S. Gumhold, and C. Rother, “Dsac - differentiable ransac for camera localization,” 2018.
- [15] E. Brachmann, T. Cavallari, and V. A. Prisacariu, “Accelerated coordinate encoding: Learning to relocalize in minutes using rgb and poses,” 2023.
- [16] T. Cavallari, S. Golodetz, N. A. Lord, J. Valentin, L. D. Stefano, and P. H. S. Torr, “On-the-fly adaptation of regression forests for online camera relocalisation,” 2017.
- [17] T. Cavallari, S. Golodetz, N. A. Lord, J. Valentin, V. A. Prisacariu, L. D. Stefano, and P. H. S. Torr, “Real-time rgb-d camera pose estimation in novel scenes using a relocalisation cascade,” *IEEE Transactions on Pattern Analysis and Machine Intelligence*, vol. 42, no. 10, p. 2465–2477, Oct. 2020. [Online]. Available: <http://dx.doi.org/10.1109/TPAMI.2019.2915068>
- [18] X. Li, S. Wang, Y. Zhao, J. Verbeek, and J. Kannala, “Hierarchical

- scene coordinate classification and regression for visual localization,” 2020.
- [19] E. Brachmann and C. Rother, “Learning less is more - 6d camera localization via 3d surface regression,” 2018.
- [20] —, “Expert sample consensus applied to camera re-localization,” 2019.
- [21] D. DeTone, T. Malisiewicz, and A. Rabinovich, “Superpoint: Self-supervised interest point detection and description,” 2018.
- [22] M. Dusmanu, I. Rocco, T. Pajdla, M. Pollefeys, J. Sivic, A. Torii, and T. Sattler, “D2-net: A trainable cnn for joint detection and description of local features,” 2019.
- [23] J. Revaud, P. Weinzaepfel, C. D. Souza, N. Pion, G. Csurka, Y. Cabon, and M. Humenberger, “R2d2: Repeatable and reliable detector and descriptor,” 2019.
- [24] P. Lindenberger, P.-E. Sarlin, and M. Pollefeys, “Lightglue: Local feature matching at light speed,” 2023.
- [25] J. Sun, Z. Shen, Y. Wang, H. Bao, and X. Zhou, “Loftr: Detector-free local feature matching with transformers,” 2021.
- [26] G. Potje, F. Cadar, A. Araujo, R. Martins, and E. R. Nascimento, “Xfeat: Accelerated features for lightweight image matching,” in *2024 IEEE / CVF Computer Vision and Pattern Recognition (CVPR)*, 2024.
- [27] P. Lindenberger, P.-E. Sarlin, V. Larsson, and M. Pollefeys, “Pixel-perfect structure-from-motion with featuremetric refinement,” 2021.
- [28] S. Chen, X. Li, Z. Wang, and V. Prisacariu, “Dfnet: Enhance absolute pose regression with direct feature matching,” in *Proceedings of the European Conference on Computer Vision (ECCV)*, 2022.
- [29] L. Yen-Chen, P. Florence, J. T. Barron, A. Rodríguez, P. Isola, and T.-Y. Lin, “Inerf: Inverting neural radiance fields for pose estimation,” 2021.
- [30] S. Chen, Z. Wang, and V. Prisacariu, “Direct-posenet: Absolute pose regression with photometric consistency,” 2021.
- [31] B. Zhao, L. Yang, M. Mao, H. Bao, and Z. Cui, “Pnerfloc: Visual localization with point-based neural radiance fields,” 2023.
- [32] Q. Zhou, M. Maximov, O. Litany, and L. Leal-Taixé, “The perfect match: Exploring nerf features for visual localization,” 2024. [Online]. Available: <https://arxiv.org/abs/2403.09577>
- [33] Y. Sun, X. Wang, Y. Zhang, J. Zhang, C. Jiang, Y. Guo, and F. Wang, “icomma: Inverting 3d gaussians splatting for camera pose estimation via comparing and matching,” 2023.
- [34] L. Yen-Chen, P. Florence, J. T. Barron, A. Rodriguez, P. Isola, and T.-Y. Lin, “Inerf: Inverting neural radiance fields for pose estimation,” in *2021 IEEE/RSJ International Conference on Intelligent Robots and Systems (IROS)*. IEEE, 2021, pp. 1323–1330.
- [35] Z. Zhu, S. Peng, V. Larsson, W. Xu, H. Bao, Z. Cui, M. R. Oswald, and M. Pollefeys, “Nice-slam: Neural implicit scalable encoding for slam,” in *Proceedings of the IEEE/CVF Conference on Computer Vision and Pattern Recognition*, 2022, pp. 12786–12796.
- [36] A. Kendall, M. Grimes, and R. Cipolla, “Posenet: A convolutional network for real-time 6-dof camera relocalization,” 2016.
- [37] Y. Shavit, R. Ferens, and Y. Keller, “Learning multi-scene absolute pose regression with transformers,” 2021.
- [38] S. Chen, T. Cavallari, V. A. Prisacariu, and E. Brachmann, “Map-relative pose regression for visual re-localization,” 2024. [Online]. Available: <https://arxiv.org/abs/2404.09884>
- [39] H. Germain, D. DeTone, G. Pascoe, T. Schmidt, D. Novotny, R. Newcombe, C. Sweeney, R. Szeliski, and V. Balntas, “Feature query networks: Neural surface description for camera pose refinement,” in *Proceedings of the IEEE/CVF Conference on Computer Vision and Pattern Recognition (CVPR) Workshops*, June 2022, pp. 5071–5081.
- [40] A. Moreau, N. Piasco, M. Bennehar, D. Tsishkou, B. Stanculescu, and A. de La Fortelle, “Crossfire: Camera relocalization on self-supervised features from an implicit representation,” 2023. [Online]. Available: <https://arxiv.org/abs/2303.04869>
- [41] A. Moreau, N. Piasco, D. Tsishkou, B. Stanculescu, and A. de La Fortelle, “Lens: Localization enhanced by nerf synthesis,” 2021.
- [42] B. Glocker, S. Izadi, J. Shotton, and A. Criminisi, “Real-time rgb-d camera relocalization,” in *International Symposium on Mixed and Augmented Reality (ISMAR)*. IEEE, October 2013. [Online]. Available: <https://www.microsoft.com/en-us/research/publication/real-time-rgb-d-camera-relocalization/>
- [43] J. L. Schönberger and J.-M. Frahm, “Structure-from-motion revisited,” in *Conference on Computer Vision and Pattern Recognition (CVPR)*, 2016.
- [44] Y. Liu, H. Guan, C. Luo, L. Fan, N. Wang, J. Peng, and Z. Zhang, “Citygaussian: Real-time high-quality large-scale scene rendering with gaussians,” *arXiv preprint arXiv:2404.01133*, 2024.
- [45] J. Lin, Z. Li, X. Tang, J. Liu, S. Liu, J. Liu, Y. Lu, X. Wu, S. Xu, Y. Yan, and W. Yang, “Vastgaussian: Vast 3d gaussians for large scene reconstruction,” in *CVPR*, 2024.